Icarus 214 (2011) 147–160

Contents lists available at ScienceDirect

Icarus

journal homepage: www.elsevier.com/locate/icarus

The origin of Vesta's crust: Insights from spectroscopy of the Vestoids

R.G. Mayne [a,b,c,*], J.M. Sunshine [d], H.Y. McSween Jr. [a], S.J. Bus [e], T.J. McCoy [b]

[a] Department of Earth and Planetary Sciences, 1412 Circle Drive, University of Tennessee, Knoxville, TN 37996-1410, United States
[b] Smithsonian Institution, National Museum of Natural History, 10th & Constitution NW, Washington, DC 20560-0119, United States
[c] School of Geology, Energy, and the Environment, Texas Christian University, TCU Box 298830, Fort Worth, TX 76129, United States
[d] Department of Astronomy, University of Maryland College Park, MD 20742-2421, United States
[e] University of Hawaii, Institute for Astronomy, Hilo, HI 96720, United States

ARTICLE INFO

Article history:
Received 6 May 2010
Revised 13 April 2011
Accepted 14 April 2011
Available online 23 April 2011

Keywords:
Asteroid Vesta
Asteroids, Surfaces
Asteroids, Composition
Spectroscopy
Meteorites

ABSTRACT

High quality VNIR spectra of 15 Vestoids, small asteroids that are believed to originate from Vesta, were collected and compared to laboratory spectra and compositional data for selected HED meteorites. A combination of spectral parameters such as band centers, and factors derived from Modified Gaussian Model fits (band centers, band strengths, calculation of the low to high-Ca pyroxene ratio) were used to establish if each Vestoid appeared most like eucrite or diogenite material, or a mixture of the two (howardite). This resulted in the identification of the first asteroid with a ferroan diogenite composition, 2511 Patterson. This asteroid can be used to constrain the size of diogenite magma chambers within the crust of Vesta. The Vestoids indicate that both large-scale homogeneous units (>5 km) and smaller-scale heterogeneity (<1 km) exist on the surface of Vesta, as both monomineralogic (eucrite or diogenite material alone) and mixed (both eucrite and diogenite) spectra are observed. The small-scale of the variation observed within the Vestoid population is predicted by the partial melting model, which has multiple intrusions penetrating into the crust of Vesta. It is much more difficult to reconcile the observations here with the magma ocean model, which would predict much more homogeneous layers on a large-scale both at the surface and with depth.

1. Introduction

The howardites, eucrites, and diogenites (HEDs) have long been spectrally associated with 4 Vesta, the second largest asteroid in the main-belt (McCord et al., 1970). The discovery of a group of small asteroids spectrally similar and dynamically linked to Vesta, called the 'Vestoids' (Binzel and Xu, 1993), supports this proposed relationship as these asteroids provide a pathway for the delivery of HED meteorites to Earth (Marzari et al., 1996). Other basaltic asteroids spectrally similar to Vesta, but outside its dynamical family (Lazzaro et al., 2000; Roig et al., 2008), have since been identified and are called V-type (e.g. Tholen and Barucci, 1989; Bus and Binzel, 2002). Here we present VIS–NIR spectra (~0.4–2.5 μm) for 14 Vestoids and 1 V-type asteroid; although we shall refer to all 15 spectra collectively as the Vestoids here for simplicity. Their spectra are modeled and compared with those for selected HED meteorites to constrain the mineralogy of each individual Vestoid and establish the variation seen within the Vestoids as a whole.

No model currently proposed for the formation of Vesta is capable of reproducing all the geochemical trends seen within the HEDs (Mittlefehldt and Lindstrom, 2003). However, the processes that produce large and small-scale igneous units are different and the Vestoids provide us with an opportunity to predict the size of igneous provinces on Vesta, thereby providing clues into its petrogenesis. The Vestoids analyzed here vary from <1 km to almost 8 km in diameter and we evaluate the most popular current models for the petrogenesis of Vesta (partial melting and a magma ocean) using evidence gleaned from the Vestoids.

2. Methodology

2.1. Collection of asteroid spectra

The VIS–NIR asteroid data were obtained in two different surveys, the Small Main-belt Asteroid Spectroscopic Survey, Phase II (SMASSII), that covers the visible region of the spectrum and a near-infrared (NIR) spectroscopic survey of asteroids, covering the wavelength interval 0.82–2.49 μm. These observations were taken at two different epochs, utilizing a total of three different telescopes. The SMASSII data were taken between February 1996 and November 1997 at the Michigan-Dartmouth-MIT (MDM) Observatory on Kitt Peak in Arizona, using both the 1.3-m

* Corresponding author at: School of Geology, Energy, and the Environment, Texas Christian University, TCU Box 298830, Fort Worth, TX 76129, United States. Fax: +1 817 257 7789.
E-mail address: r.g.mayne@tcu.edu (R.G. Mayne).

0019-1035/$ - see front matter © 2011 Elsevier Inc. All rights reserved.
doi:10.1016/j.icarus.2011.04.013

McGraw-Hill and 2.4-m Hiltner telescopes. The NIR data were taken between October 2000 and July 2005 with the NASA Infrared Telescope Facility (IRTF), a 3.0-m telescope on Mauna Kea in Hawaii.

The SMASSII survey utilized a low-resolution grism spectrograph that worked in combination with one of two CCD camera systems. These two cameras, one consisting of a SITE 1024×1024 thinned, backside illuminated CCD with 24-μm, and the other a Loral 2048×2048 thick, frontside-illuminated CCD with 15-μm pixels, were each binned on readout to produce a spatial resolution (along the length of the slit) of abut 0.5 arcsec per pixel. All visible spectra were taken with a 4.5 arcsec-wide slit, producing a spectral resolving power of $R \sim 100$ ($\lambda/\Delta\lambda$). Details of the SMASSII observations and data reduction methods can be found in Bus and Binzel (2002).

The NIR data were taken with SpeX, the low- to medium-resolution spectrograph and imager at the NASA IRTF. The spectrograph portion of this instrument uses a Raytheon Aladdin 3 1024×1024 pixel InSb array with 27-μm pixels. For the asteroid observations, SpeX was used in the low-resolution prism mode with a 0.8 arcsec slit. This produced a spatial image scale of 0.15 arcsec per pixel, and a spectral resolving power of about $R \sim 100$, comparable to that of the SMASSII results. Further details on the instrumentation used in the SpeX asteroid survey can be found in Rayner et al. (2003). Details of observing strategy, data reduction, and calibration procedures used in the SpeX survey are outlined in more detail in Sunshine et al. (2004).

The data from both surveys were completely reduced and extracted to 1-D spectra and calibrated as relative reflectance versus wavelength. Observational circumstances for each of the spectra presented here are given in Table 1. Combination of the visible and NIR spectra relied on the overlap region from 0.82 to 0.92 μm that was sampled in both datasets. Since the spectra in both surveys were binned/resampled at uniform wavelengths (using a dispersion of 0.005 μm per channel), there are (at most) 21 points that overlap between the visible and near-IR. Each NIR spectrum was scaled to match the corresponding VIS spectrum (which is been normalized to unity at 0.55 μm) using a mean scaling factor determined from those 21 overlap points.

There are 15 V-type asteroids, not including Vesta, that have been observed so far in the NIR asteroid survey. This survey is designed to sample representative asteroids of all taxonomic types, and is not focused just on V-types or Vestoids. Of the V-types observed, only one (3908 Nyx) is a planet crossing asteroid. Therefore in this study we present the spectra of 14 "Vestoids", i.e.: dynamically related members of the Vesta family, and one planet crossing V-type asteroid. The asteroids targeted in these spectroscopic surveys were identified by Zappalà et al. (1995) as belonging to the Vesta dynamical family. Based on the Zappalà et al. (1995) results, the Vesta family was estimated to have 372 members. However, the number of Vesta family members is constantly increasing as the total number of known asteroids grows. Nesvorny et al. (2006) recognized 5575 asteroids as belonging to the Vesta dynamical family.

2.2. Temperature effects

Hinrichs et al. (1999) calculated that the surface temperature of an asteroid at Vesta's position in the main-belt (2.36 AU) will be ~200 K, if a fine-grained regolith is present. Laboratory spectra are commonly collected at room temperature ~293 K. It has been demonstrated that absorption band positions of silicate minerals vary with temperature (e.g. Singer and Roush, 1985; Roush and Singer, 1987; Schade and Wäsch, 1999a; Moroz et al., 2000). However, all current temperature corrections are based on data for pyxoxenes of a terrestrial composition. Vestoid mineralogy is expected to reflect that of the HED meteorites (e.g. Binzel and Xu, 1993), which are a mixture of different pyroxenes (orthopyroxene, pigeonite, and augite), plagioclase, and other minor phases such as SiO_2, chromite, ilmenite, olivine, FeNi metal, and sulfides. The pyroxenes they contain are also Fe-rich compared to the terrestrial pyroxenes used in temperature correction calibration studies such as Roush and Singer (1987). No study has focused on the movement of absorption band positions of the HEDs as a function of temperature.

Burbine et al. (2001) reported the band center positions of several eucrite and howardite spectra collected at 200 K and 300 K. Their results show no consistent band center movement with temperature change. For example, EET 83251 at 200 K had a B1 position at 0.93 μm, and B2 at 1.97 μm. The temperature-dependent wavelength correction as given by Burbine et al. (2009) predicts a shift of 0.002 μm for this meteorite in the B1 region and a 0.014 μm in B2. However, that does not accurately predict what was measured. At 300 K EET 83251 had a B1 position of 1.94 μm (a 0.01 μm shift) and B2 of 1.97 μm (no change). There is no temperature correction currently available that accurately reflects the behavior of HED, and therefore Vestoid, spectra with changing temperature. As a result, no temperature correction has been applied to the data presented here.

2.3. Collection of laboratory spectra

VIS–NIR (0.3–2.55 μm) spectra for howardites, eucrites, and diogenites were collected using the Bi-directional Reflectance Spectrometer at the NASA/Keck Reflectance Experiment Laboratory (RELAB) at Brown University (Pieters, 1983; Pieters and Hiroi, 2004). This research utilizes spectra for eight unbrecciated eucrites (ALH A81001, BTN 00300, Chervony Kut, EET 87520, GRA 98098, MET 01081, MAC 02522, and PCA 91078), which were presented in Mayne et al. (2010). All other HED spectra were available for download and were acquired by Hiroi and Pieters at the NASA RELAB facility.

2.4. VIS–NIR spectroscopy and modeling

Band centers of the HED and Vestoid spectra were calculated for the 1 and 2-μm regions using the method of Gaffey et al. (1993). The resulting band centers shall be referred to as 'continuum-removed band centers' throughout the rest of this paper. The errors for the continuum-removed band centers were calculated using a method similar to that of Storm et al. (2007), as described in Burbine et al. (2009). The reflectance values for each continuum-removed band were resampled randomly using a Gaussian distribution for the observational error. The resulting values were fit with a second-order polynomial and the band center determined. This was repeated a total of 100 times and the band center values were averaged and the standard deviation was calculated.

All HED and Vestoid spectra were also fit using the Modified Gaussian Model (MGM) (Sunshine et al., 1990; Sunshine and Pieters, 1993). Data for the MGM fits are presented below, with the exception of the unbrecciated eucrites spectra, which are presented in Mayne et al. (2010).

MGM models each spectrum as a continuum and a series of modified Gaussian distributions, with each distribution representing a specific absorption feature characterized by three parameters: band strength, band center, and band width (Sunshine et al., 1990). Band center values produced by MGM will be referred to hereafter as 'MGM-derived band centers'. This approach has been shown to successfully resolve the absorptions of overlapping bands (Mustard, 1992; Sunshine and Pieters, 1993; Schade and Wäsch, 1999b; Sunshine et al., 1990, 2004; Kanner et al., 2007; Klima et al., 2007, 2008), such as those seen in the HED and Vestoid spec-

Table 1
Observational data for Vestoid spectra.

Asteroid	Spectral range	UT date	Exposure (s)	Mean airmass	Precipitable water (mm)	Heliocentric distance (AU)	Phase angle (°)	*V* magnitude
1929 Kollaa	VIS	22–February–1997	1800	1.06		2.18	19.3	15.6
	NIR	19–February–2001	1440	1.04	0.9	2.21	14.4	15.3
2045 Peking	VIS	23–November–1997	1800	1.13		2.51	18.6	16.4
	NIR	14–January–2002	2400	1.02	4.7	2.48	21.7	16.7
2511 Patterson	VIS	15–April–1997	1800	1.07		2.27	15.0	15.8
	NIR	07–May–2004	1920	1.04	1.3	2.23	21.2	16.1
2566 Kirghizia	VIS	26–November–1996	1800	1.08		2.43	12.8	16.2
	VIS	30–November–1996	1800	1.08		2.42	14.3	16.3
	NIR	08–May–2002	1920	1.12	2.5	2.41	9.8	16.0
2579 Spartacus	VIS	30–April–1996	2700	1.57		2.09	10.9	15.5
	NIR	10–October–2000	1680	1.15	1.2	2.22	18.9	16.4
2653 Principia	VIS	13–April–1997	2700	1.56		2.43	19.6	16.2
	NIR	26–November–2002	2880	1.13	4.4	2.53	17.8	16.3
	NIR	16–July–2005	1680	1.24	1.5	2.59	3.1	15.5
2763 Jeans	VIS	23–November–1997	1800	1.19		1.96	28.0	16.0
	NIR	26–June–2004	1920	1.44	3.6	2.24	12.6	15.7
2795 Lepage	VIS	9–September–1996	1800	1.06		2.33	20.4	17.0
	NIR	09–April–2005	1440	1.16	0.9	2.26	4.7	15.9
2851 Harbin	VIS	29–April–1996	1800	1.57		2.77	5.4	16.2
	NIR	24–August–2001	1680	1.30	2.0	2.42	8.7	15.6
	NIR	12–January–2003	2880	1.03	1.3	2.20	16.0	15.9
2912 Lapalma	VIS	17–January–1997	1800	1.04		2.29	17.5	16.3
	NIR	20–February–2001	1920	1.01	0.9	2.14	8.7	15.3
3155 Lee	VIS	12–April–1997	1800	1.40		2.54	4.0	16.0
	NIR	22–June–2001	1680	1.59	2.9	2.56	8.4	16.2
	NIR	14–July–2005	1680	1.56	2.3	2.43	7.9	15.9
3782 Celle	VIS	13–September–1997	1800	1.28		2.39	10.7	15.9
	NIR	26–November–2002	1920	1.03	5.5	2.60	17.1	16.8
	NIR	25–June–04	1680	1.38	3.9	2.19	13.3	15.5
3908 Nyx	VIS	09–September–1996	1800	1.25		1.15	30.2	15.1
	VIS	12–October–1996	900	1.07		1.05	48.5	13.9
	NIR	26–November–2004	3120	1.22	2.2	1.44	3.7	16.7
	NIR	11–September–2004	1920	1.18	1.4	1.17	46.1	16.6
4188 Kitezh	VIS	08–February–1996	1800	1.16		2.55	0.4	15.8
	NIR	14–August–2001	1680	1.29	1.5	2.10	10.8	15.3
4215 Kamo	VIS	08–April–1997	2700	1.77		2.34	16.5	16.0
	NIR	11–November–2002	3840	1.03	5.3	2.52	17.3	16.5
	NIR	15–July–2005	2400	1.23	2.9	2.51	3.2	15.6

Spectral range: Visible spectra cover 0.44–0.92 μm, and were taken with either the 1.3-m or 2.4-m telescope at MDM observatory on Kitt Peak using a low-resolution grism spectrograph with CCD camera. Near-IR spectra cove 0.82–2.42 μm and were taken with the 3.0-m NASA IRTF on Mauna Kea using SpeX.
Amount of precipitable water above Mauna Kea was determined from fits to telluric water absorption bands in the SpeX data using the ATRAN (Atomospheric TRANsmission) modeling routine (Lord, 1992) that utilizes the HITRAN (HIgh resolution TRANsmission) database (Rothman et al., 2005).

tra. Three diogenite (EET A79002, LAP 91900, GRO 95555) and howardite (EET 87503, QUE 94200, Y-791573) spectra were fit using MGM. These samples were selected because there was previously published data on their pyroxene compositions. The results of MGM were then used to estimate the relative proportions of LCP and HCP from the spectra that required a two-pyroxene model (e.g. Sunshine and Pieters, 1993; Sunshine et al., 2004; Kanner et al., 2007).

The fit of an MGM model will always improve with a greater number of bands, because the model then has more Gaussian distributions with which to model the spectrum. Therefore, it is extremely important when using MGM to start to fit each spectrum with the minimum number of bands (Gaussian distributions) that you believe may explain its absorption features. In this study, each spectrum was first modeled as one pyroxene, whose composition was allowed to vary, because that is the simplest HED-like mineralogy. The MGM outputs a wavelength dependent RMS error and this shows characteristic features (peak errors offset from band centers) that are diagnostic of missing bands (Sunshine and Pieters, 1993). If these errors were observed then the spectrum was modeled using a two-pyroxene model, consisting of one low-Ca pyroxene and one high-Ca pyroxene. Additional bands were only added if the RMS error indicated that they were required.

2.5. Calculation of Vestoid size

The diameter of an asteroid can be estimated from its absolute magnitude (H) and its geometric albedo (p_v) (Chesley et al., 2002):

$$D \approx 1329\ \text{km} \times 10^{-H/5} p_v^{-1/2} \quad (1)$$

In this study we adopt the practice used by previous studies of the Vestoids (e.g. Burbine et al., 2001) and take the value of the geometric albedo to be 0.42 for all Vestoids, which is the value derived for Vesta based on Infrared Astronomical Satellite (IRAS) measurements. All of the Vestoids analyzed here lie between 4.7 and 7.8 km in diameter, with the exception of 3908 Nyx, which is 0.7 km. If the visual albedo value used to calculate the diameter is incorrect by up to a factor of 2 (actual value lies between 0.21 and 0.84) then the largest, 7.8 km diameter asteroid, could actually

lie between 5.5 and 11.0 km and the smallest, 3908 Nyx, between 0.5 and 1.0 km.

3. Results

3.1. HED pyroxene compositions

Compositional data for the pyroxenes in the howardites, eucrites, and diogenites that were fit using MGM are presented in Table 2. The three diogenites contain one-pyroxene of a low-calcium composition (Wo_2). They are magnesium rich in comparison to the eucrites (diogenites pyroxenes have En_{74-76} compared to En_{21-56} for all eucrite pyroxenes). The howardites, as breccias, contain a wide range of pyroxene compositions, the end-members of which are given in Table 2. The LCP end-member composition for the howardites is similar to that of the diogenites; however only one of the three howardites (Y-791573) has a HCP composition that extends to calcium compositions seen within the HCP in the eucrites.

3.2. Spectral modeling

The spectra of all HEDs and Vestoids are dominated by the characteristic 1 and 2-μm pyroxene absorption features (Figs. 1–4). Continuum-removed band centers for the HEDs and Vestoids, and MGM-derived band centers and band strengths for the spectra that were modeled, are given in Tables 3 and 4. Continuum-removed band 2 (~1 μm) versus band 1 (~2 μm) center positions for all HED spectra presented in this paper are shown in Fig. 5a. As expected, all eucrite spectra have continuum-removed band centers at comparatively long wavelengths (reflecting high modal abundance of HCP), and diogenite spectra at short wavelengths, with the howardites bridging the gap between the two. The majority of the Vestoids studied here have band centers that overlap the field defined by howardites (Fig. 5b), suggesting that they reflect a mixture of diogenite and eucrite materials.

The three diogenite spectra selected were all well fit with MGM using a one-pyroxene model (Tables 3 and 5). The diogenite models all show a non-random residual error in the 1-μm region, with the peak error occurring at the same wavelength as the modeled band center (Fig. 6). This is likely to be due to band saturation rather than missing absorption bands, which are offset and much larger (Sunshine and Pieters, 1993). All howardite spectra required a two-pyroxene model to achieve a good fit (Tables 3 and 5, Fig. 6). All eucrite spectra were modeled by Mayne et al. (2010) and the resulting model parameters are given in Table 3. Three examples of MGM fits for the eucrites are given in Fig. 6.

The majority of the Vestoids required two-pyroxene fits (Table 4, Fig. 7), with the exception of 3155 Lee, 3782 Celle, 2851 Harbin, 4215 Kamo, and 2511 Patterson which were fit using just one low-Ca pyroxene. The ability to model these spectra with only one low-Ca pyroxene suggests a predominantly diogenite composition. 3155 Lee and 3782 Celle were best modeled using one low-Ca pyroxene with an extra band to account for the M1 absorption in the 1-μm region (Tables 4 and 5). This band is a result of Fe^{2+} in the M1 octahedral site (Burns, 1993). It is often masked by the larger M2 band in the same wavelength space. While this additional band is not required in all MGM models for the HEDs it is relatively common, with several eucrites (Chervony Kut, BTN 00300, and MAC 02522) requiring it, as well as the hypersthene within the Johnstown diogenite (Mayne et al., 2010).

The relative strengths of the LCP and HCP MGM-derived bands at both 1 and 2 μm can be used to estimate the proportion of high-calcium pyroxene in the sample, if a two-pyroxene model is needed. The estimated modes can then be compared to actual HCP and LCP modes measured for the eucrite meteorites (Mayne et al., 2010), to assess the accuracy of this calculation for the HEDs and Vestoids. HCP and LCP modes are meaningless for howardite

Table 2
Pyroxene compositions of the howardites and the diogenites modeled using MGM.

		LCP			HCP		
		Wo	En	Fs	Wo	En	Fs
Howardites*	EET 87503[a]	2	75	23	12	38	50
	QUE 94200[b]	1	81	18	11	46	43
	Y-791573[c]	2	83	15	44	48	8
Eucrites**	ALH A81001	1	41	58	43	32	25
	BTN 00300	8	36	57	39	29	32
	Chervony Kut	3	35	62	42	29	29
	EET 87520	7	37	57	40	30	30
	GRA 98098	7	36	58	21	33	46
	Ibitira	6	39	55	39	32	30
	MAC 02522***	13	32	55			
	MET 01081	6	36	58	35	31	34
	Moore County	6	47	48	42	36	22
	PCA 91078	5	36	59	41	30	30
	Serra de Mage	2	56	42	45	39	15

		Pyroxene composition		
		Wo	En	Fs
Diogenites	EET A79002[d]	2	76	22
	LAP 91900[e]	2	75	23
	GRO 95555[f]	2	74	24

All eucrite compositions are given in Mayne et al. (2009).
* The pyroxene compositions given for the howardites represent the end-members of the range seen within the sample as opposed to discrete separate compositions.
** All eucrite compositions given here are the average of analyses taken by Mayne et al. (2009).
*** MAC 02522 does not contain two separate pyroxenes and the value given here is the average of all analyses from Mayne et al. (2009).
[a] *Antarctic Meteorite Newsletter 11(2)* (1988).
[b] *Antarctic Meteorite Newsletter 18(2)* (1995).
[c] *Meteorite Newsletter J9(1)* (2000).
[d] *Antarctic Meteorite Newsletter 3(3)* (1980).
[e] *Antarctic Meteorite Newsletter 15(2)* (1992).
[f] *Antarctic Meteorite Newsletter 19(2)* (1996).

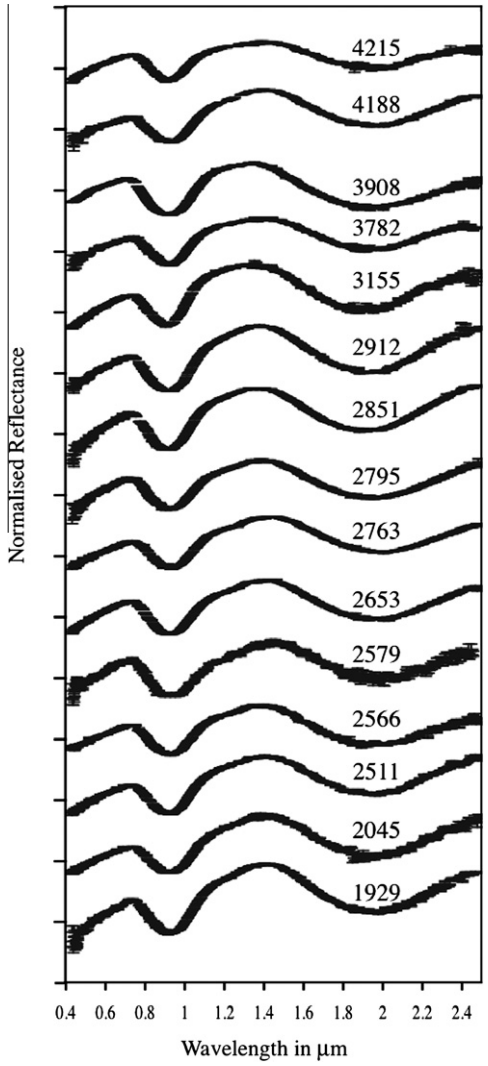

Fig. 1. The VIS–NIR reflectance spectra of all 15 Vestoids studied in this paper. The spacing between two tick marks on the *y*-axis is equal to a ΔR (reflectance) value of 1. Spectra are offset by a value of 1 for clarity. Error bars are shown on spectra.

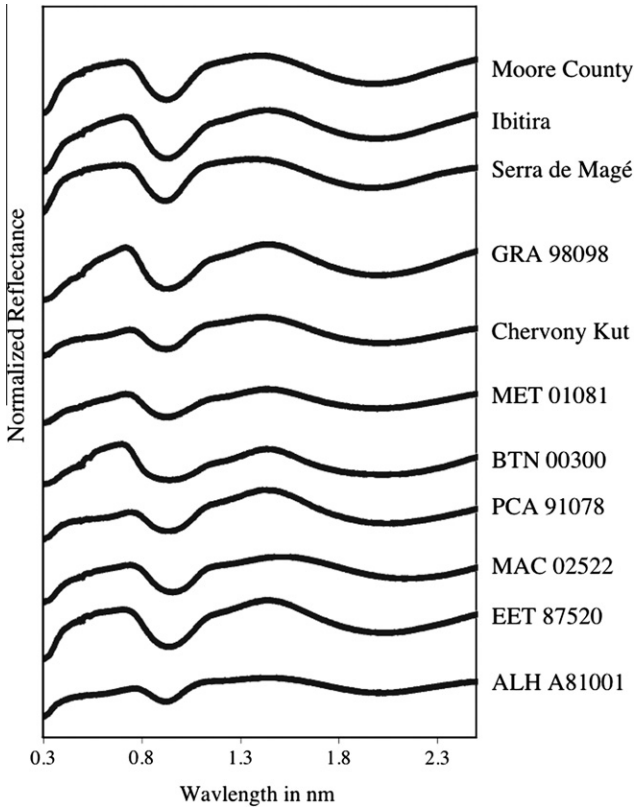

Fig. 2. The VIS–NIR reflectance spectra of the unbrecciated eucrites. The spacing between two tick marks on the *y*-axis is equal to a ΔR (reflectance) value of 1. Spectra are offset by a value of 1 for clarity. Spectra are taken from Mayne et al. (2010).

samples as they are breccias, making representative analyses almost impossible, and diogenites contain only one pyroxene. Estimates of high-calcium pyroxene abundance from the relative band strengths are within ±9% (1σ) of the actual values based upon previously collected data on the unbrecciated eucrites (Mayne et al., 2009). The HCP calculation yields similar values for all of the Vestoids. 2579 Spartacus and 2763 Jeans have the largest proportion of high-calcium pyroxene (using the value estimated from their 1-μm band) of 59% and 57% respectively, giving them similar abundances to that of the basaltic eucrites (Tables 3 and 4). All other HCP values correspond to the range shown by the selected howardites and cumulate eucrites.

4. The mineralogy of Vestoids

4.1. Mineralogic variation among the Vestoids

The Vestoids have been observed in previous studies to have spectral characteristics consistent with surface compositions of both the eucrites and howardites (Burbine et al., 2001). The mineralogical interpretations made below take into account the errors calculated for the Vestoid band center positions (Table 6). Our analyses of the Vestoid spectra indicate clear compositional differences, most likely reflecting different lithologies on or near the surface of their parent asteroid, Vesta. No evidence was found for mineralogies that were not HED in nature. This agrees with the findings of Moskovitz et al. (2010), who analyzed 39 V-type asteroids in the inner main-belt. Of the 15 Vestoid spectra presented here there appear to be seven asteroids that consist entirely of either eucrites or diogenites. 2579 Spartacus and 2763 Jeans are most likely eucrite material as they have 1 and 2-μm band centers at long wavelengths, overlapping those of the eucrite meteorite samples. In addition, a large proportion (60%) of the pyroxene in 2579 Spartacus is calculated to be of high-calcium composition. The paucity of eucrite-dominated Vestoids in this study is surprising considering how abundant eucrites are in the HED suite of meteorites.

3155 Lee, 2851 Harbin, 3782 Celle, and 4215 Kamo have continuum-removed band centers equivalent to those of normal diogenites. They are all fit well with a one-pyroxene model that is low-calcium in composition, which in petrologic terms confirms their classification as diogenites. 2511 Patterson is also fit with a one low-Ca pyroxene model but lies at longer wavelengths than the other Vestoids with diogenite compositions. Asteroid 2511 Patterson likely consists of diogenite with an Fs-rich pyroxene composition. This conclusion is supported when 2511 Patterson is compared with Y-75032, a ferroan diogenite. Y-75032 has been identified as one of the most ferroan diogenites (Yamagchi et al., 2009) and it has continuum-removed band centers at much longer wavelengths than most diogenites (Fig. 5). 2511 Patterson has continuum removed band centers that lie between that of the ferroan diogenite Y-75032 and the other 'normal' diogenites plotted here. This is the first asteroid that has been identified with a ferroan

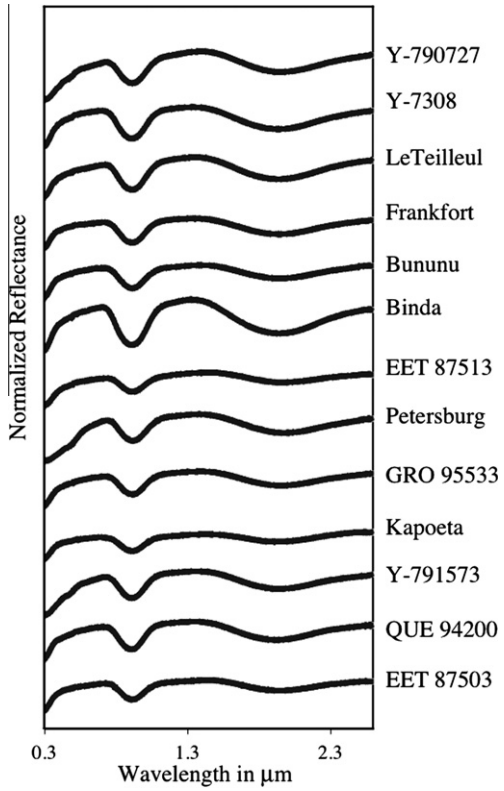

Fig. 3. The VIS–NIR reflectance spectra of all the howardites used in this study. The spacing between two tick marks on the *y*-axis is equal to a ΔR (reflectance) value of 1. Spectra are offset for clarity by a value of 1. These spectra were available for download from the RELAB database.

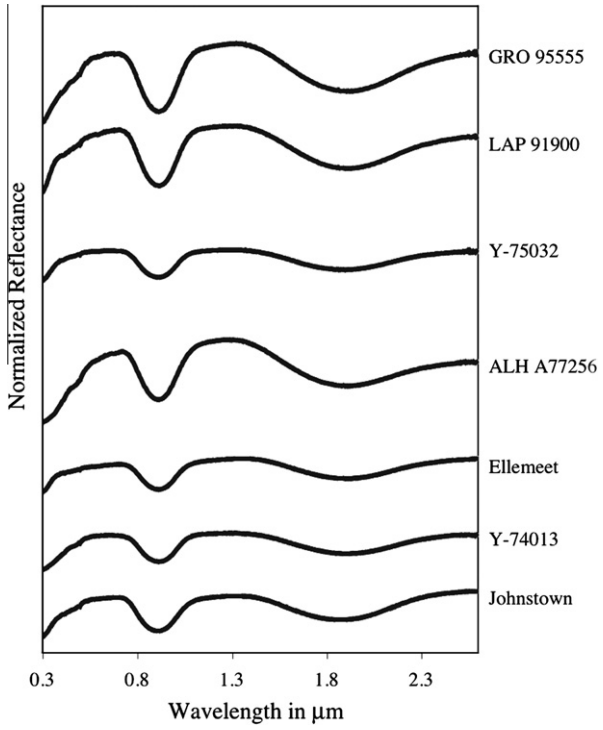

Fig. 4. The VIS–NIR reflectance of the diogenites used in this study. The spacing between two tick marks on the *y*-axis is equal to a ΔR (reflectance) value of 0.5. Spectra are offset by a value of 1 for clarity. All spectra were available for download from the RELAB database.

diogenite composition, the implications of which will be discussed later in this paper.

3908 Nyx has amongst the shortest continuum-removed band centers of the Vestoids, suggestive of a diogenite lithology. When fit with MGM 3908 Nyx requires a two-pyroxene model with an estimated LCP:HCP ratio of 70:30, more akin to that of a howardite. The LCP MGM-derived band centers for 3908 Nyx are the lowest for any Vestoid fit in this study, whereas the corresponding HCP values are similar to the other Vestoids. Therefore, the LCP MHM derived bands drive the overall continuum-removed band centers to shorter wavelengths. This suggests that the short wavelength continuum-removed band centers are a result of compositional differences between the LCP component within 3908 Nyx and the other Vestoids (e.g. 3908 Nyx may have relatively Fs-poor orthopyroxene).

The remaining eight Vestoids appear to represent mixtures of both eucrite and diogenite materials. 1929 Kollaa has previously been suggested to have compositional characteristics similar to those of cumulate eucrites (Kelley et al., 2003). However, the spectra of howardites and cumulate eucrites are similar (Burbine et al., 2009). As mentioned above, both contain a 1.2-μm feature that, though present, is often not visible to the naked eye. Cumulate eucrites contain pyroxenes with composition lower in iron, which give them shorter wavelength band centers, the same effect that the addition of low-calcium pyroxene (diogenite) would have on a basaltic eucrite. This results in overlap between the band centers of howardites and cumulate eucrites, and asteroids that also have band center values close to this region could consist of either material (see Fig. 5). Only two cumulate eucrite spectra are included here, so their band center range is not well defined. More work should be done on the spectral differences between these two groups before conclusions can be drawn as to whether any of these asteroids are dominated by cumulate eucrites.

4.2. The question of olivine-rich Vestoids

Gaffey (1997) produced a mineralogic map of the surface of Vesta, using sub-hemispheric spectral and color variations. He was able to observe eucrite and diogenite-like areas, as well as a possible olivine-bearing unit. Higher resolution Hubble Space Telescope images supported this conclusion as in the postulated 'olivine-bearing' localities Binzel et al. (1997) observed that the 1-μm band was broader and deeper than elsewhere on the surface, a diagnostic property of olivine. In recent years, the number of olivine-bearing diogenites has also increased, lending weight to the theory that that excavation on the surface of Vesta may have penetrated the uppermost mantle (e.g. Binzel et al., 1997; Gaffey, 1997; Thomas et al., 1997).

Previous authors have investigated the effect of olivine on pyroxene–olivine spectral mixtures (e.g. Cloutis et al., 1986; Gaffey et al., 2002). In spectra reflecting a mixture of LCP and olivine compositions the BAR (ratio of the area of band 2 to the area of band 1) can be used to estimate the amount of olivine (Cloutis et al., 1986). Duffard et al. (2004) used the BAR method outlined in Gaffey et al. (2002) to investigate the evidence for olivine in Vestoid spectra and concluded that five asteroids (2763 Principia, 2851 Harbin, 2045 Peking, 4796 Castalia, and 4815 Anders) that had olivine abundances of around 30%. However, as even Duffard et al. (2004) acknowledge, this method does not work in the presence of HCP. HCP is a significant modal component in the eucrites and, therefore, is also abundant in howardites, depending on the rock-types that make up that particular breccia. It does not, therefore, seem possible to apply these equations to the Vestoids at all. Any olivine abundance estimated from HED or Vestoid spectra from BAR calculations is not robust. Therefore, estimation of olivine abundances from the BAR values of Vestoid spectra will not be used here.

Table 3
Continuum-removed bands 1 and 2 centers, BARs, and MGM-derived band centers and band strengths for the HEDs.

Meteorite type	ALH A81001 Eucrite	BTN 00300 Eucrite	Chervony Kut Eucrite	EET 87520 Eucrite	GRA 98098 Eucrite	Ibitira Eucrite	MAC 02522 Eucrite	MET 01081 Eucrite	Moore Country Cumulate Eucrite	PCA 91078 Eucrite	Serra de Mage Cumulate Eucrite	EET 87503 Howardite	QUE 94200 Howardite	Y-791573 Howardite	EETA 79002 Diogenite	LAP 91900 Diogenite	GRO 95555 Diogenite
Continuum removed band centers (μm)																	
Band 1	0.938	0.951	0.938	0.953	0.944	0.942	0.971	0.942	0.938	0.956	0.931	0.930	0.924	0.928	0.919	0.921	0.922
Band 2	2.014	2.011	2.006	2.016	2.007	1.997	2.127	1.995	1.986	2.020	1.969	1.956	1.927	1.947	1.895	1.909	1.910
BAR	1.639	1.154	2.394	1.351	1.337	1.289	1.176	1.460	1.604	2.152	1.694	1.582	2.034	1.986	1.897	1.840	1.917
MGM band centers (μm)																	
1 μm M1		0.833	0.872				0.884										
LCP at 1		0.908	0.921	0.896	0.898	0.903		0.899	0.906	0.893	0.919	0.920	0.917	0.918	0.917	0.918	0.918
HCP at 1	0.933	1.013	0.986	1.007	1.014	1.007	0.988	1.010	0.993	1.010	0.995	1.032	1.000	1.005			
1.2 feature	1.190	1.212	1.192	1.203	1.197	1.201	1.123	1.208	1.177	1.204	1.166	1.234	1.180	1.194	1.171	1.171	1.163
LCP at 2		1.806	1.909	1.907	1.899	1.927		1.893	1.932	1.891	1.936	1.931	1.907	1.922	1.896	1.914	1.912
HCP at 2	2.024	2.198	2.219	2.239	2.120	2.210	2.154	2.215	2.232	2.236	2.243	2.084	2.154	2.215			
MGM band strengths (log reference)																	
Extra M1		−0.561	−0.258				−0.360										
LCP at 1		−0.886	−0.505	−0.740	−1.029	−0.782		−0.919	−0.770	−0.877	−0.579	−0.532	−0.732	−0.711	−1.112	−1.098	−1.143
HCP at 1	−0.538	−0.977	−0.368	−0.608	−0.634	−0.499	−0.901	−0.577	−0.398	−0.670	−0.096	−0.103	−0.071	−0.091			
1.2 Feature	−0.093	−0.727	−0.197	−0.259	−0.341	−0.211	−0.225	−0.337	−0.153	−0.338	−0.065	−0.093	−0.087	−0.091	−0.097	−0.101	−0.122
LCP at 2		−0.949	−0.567	−0.485	−0.570	−0.434		−0.585	−0.492	−0.616	−0.400	−0.273	−0.452	−0.424	−0.742	−0.696	−0.713
HCP at 2	−0.349	−0.978	−0.408	−0.373	−0.398	−0.200	−0.370	−0.380	−0.171	−0.556	−0.093	−0.068	−0.068	−0.085			
% HCP from 1[a]		73	61	65	55	56		55	47	63	18	20	14	16			
% HCP from 2[a]		71	61	63	59	44		57	35	67	25	26	19	22			
MGM band widths (μm)																	
Extra M1							0.140										
LCP at 1	0.000	0.198	0.194	0.188	0.182	0.181		0.187	0.190	0190	0.194	0.170	0.180	0.180	0.180	0.190	0.200
HCP at 1	0.188	0.201	0.182	0.184	0.173	0.185	0.187	0.190	0.183	0.177	0.188	0.210	0.190	0.200			
1.2 feature	0317	0.318	0.281	0.284	0.307	0.283	0.338	0.290	0.280	0.285	0.279	0.320	0.300	0.310	0.330	0.300	0.290
LCP at 2	0.000	0.582	0.562	0.553	0.567	0.559		0.565	0.558	0.554	0.565	0.590	0.580	0.580	0.570	0.620	0.620
HCP at 2	0.597	0.565	0.562	0.563	0.562	0.561	0.704	0.564	0.564	0.563	0.564	0.570	0.570	0.570			

[a] These values denote the percentage pyroxene that has a high-calcium composition estimated to be in the material measured. This is estimated using the relative strengths of the LCP and HCP bands in both the 1 and 2 μm regions using the method outlined by Sunshine and Pieters (1993).

Table 4
Continuum-removed bands 1 and 2 centers, BARs, and MGM-derived band centers and strengths for the Vestoids.

	1929 Kollaa	2045 Peking	2511 Patterson	2566 Kirghizia	2579 Spartacus	2653 Principia	2763 Jeans	2795 Lepage	2851 Harbin	2912 Lapalma	3155 Lee	3782 Celle	3908 Nyx	4188Kitezh	4215Kamo
Continuum removed band centers (μm)															
Band 1	0.935	0.936	0.929	0.933	0.940	0.934	0.940	0.933	0.923	0.926	0.915	0.927	0.924	0.934	0.925
Band 2	1.940	1.950	1.942	1.938	1.985	1.951	1.976	1.946	1.915	1.928	1.896	1.923	1.926	1.942	1.930
BAR	2.098	2.511	2.441	2.108	1.635	1.970	2.104	2.325	2.331	2.395	2.688	1.883	2.134	2.171	1.820
MGM band centers (μm)															
1 μm Ml											0.840	0.879			
LCP at 1	0.908	0.909	0.916	0.903	0.888	0.912	0.911	0.900	0.910	0.892	0.926	0.940	0.876	0.892	0.914
HCP at 1	0.986	0.991		0.983	1.003	1.004	0.994	0.989		0.973			0.990	0.978	
1.2 feature	1.186	1.185	1.178	1.176	1.184	1.171	1.187	1.168	1.163	1.161	1.136	1.146	1.119	1.173	1.154
LCP at 2	1.904	1.911	1.939	1.900	1.933	1.912	1.931	1.890	1.907	1.907	1.899	1.937	1.852	1.902	1.937
HCP at 2	2.280	2.279		2.246	2.271	2.270	1.271	2.262		2.275			2.186	2.268	
MGM relative strengths (log reflectance)															
Extra M1											−0.268	−0.359			
LCP at 1	−0.809	−0.719	−0.881	−0.643	−0.639	−0.764	−0.602	−0.615	−0.972	−0.800	−0.361	−0.365	−0.807	−0.597	−0.627
HCP at 1	−0.156	−0.124		−0.186	−0.441	−0.121	−0.181	−0.206		−0.249			−0.403	−0.232	
1.2 feature	−0.214	−0.194	−0.193	−0.188	−0.228	−0.210	−0.184	−0.188	−0.200	−0.185	−0.172	−0.141	−0.193	−0.189	−0.142
LCP at 2	−0.606	−0.575	−0.558	−0.608	−0.490	−0.584	−0.480	−0.563	−0.651	−0.650	−0.622	−0.503	−0.665	−0.517	−0.427
HCP at 2	−0.197	−0.147		−0.200	−0.175	−0.181	−0.170	−0.208		−0.082			−0.340	−0.166	
% HCP from 1[a]	20	19		28	59	18	29	32		30			46	37	
% HCP from 2[a]	33	27		33	36	31	35	37		17			48	32	
MGM band widths (μm)															
Extra Ml											0.240	0.250			
LCP at 1	0.250	0.250	0.240	0.230	0.180	0.220	0.220	0.220	0.240	0.240	0.190	0.180	0.150	0.250	0.210
HCP at 1	0.200	0.200		0.190	0.180	0.200	0.200	0.200		0.190			0.280	0.190	0.310
1.2 feature	0.290	0.290	0.290	0.280	0.270	0.290	0.290	0.280	0.300	0.270	0.310	0.320	0.590	0.280	
LCP at 2	0.590	0.590	0.620	0.600	0.550	0.590	0.590	0.600	0.630	0.580	0.610	0.600	0.580	0.600	0.610
HCP at 2	0.600	0.600		0.600	0.580	0.600	0.600	0.600		0.600				0.600	

[a] These values denote the percentage pyroxene that has a high-calcium composition estimated to be in the material measured. This is estimated using the relative strengths of the LCP and HCP bands in both the 1 and 2 μm regions using the method outlined by Sunshine and Pieters (1993).

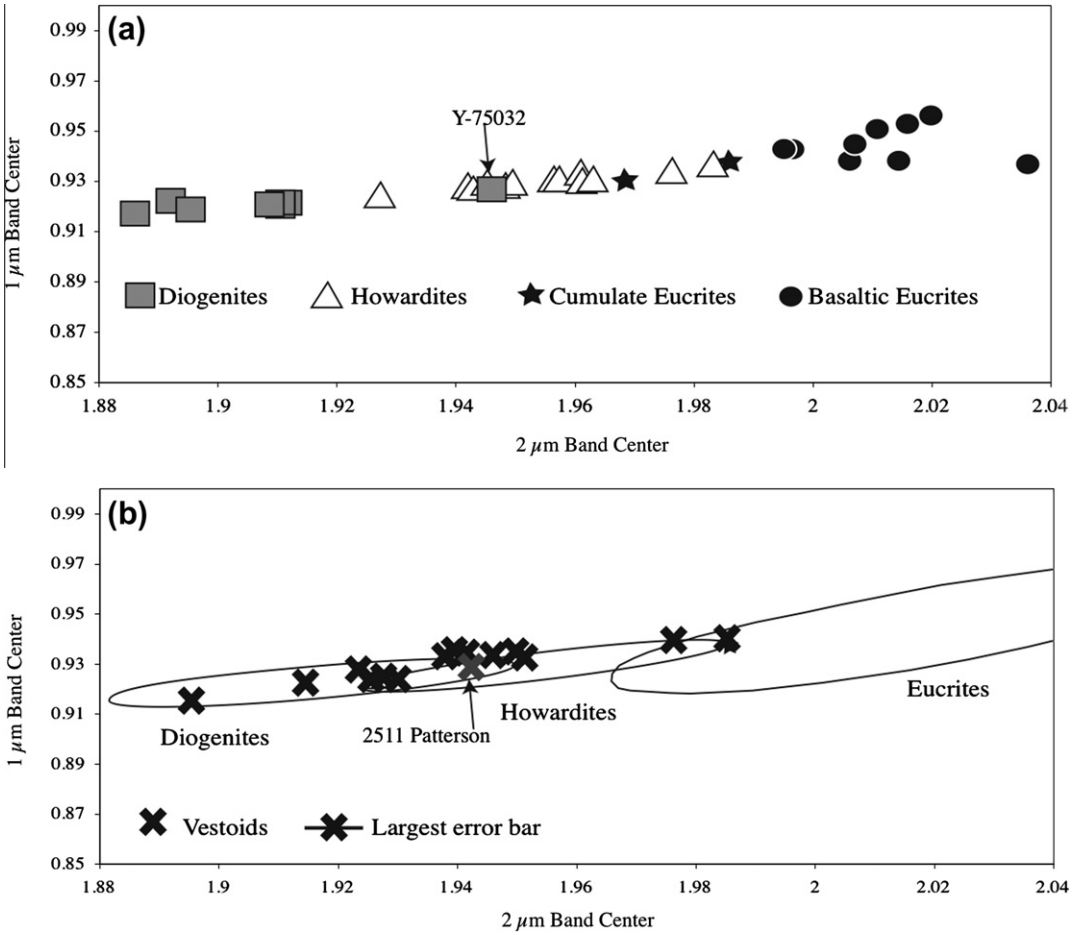

Fig. 5. Continuum-removed band centers for Vestoids and HED spectra. (a) Continuum-removed band centers for the HEDs. The band positions for Y-75032 are highlighted in this figure. Y-75032 is a ferroan diogenite and has band centers at much longer wavelengths than those of the more common Mg-rich diogenites. (b) Continuum-removed band centers for the Vestoids, superimposed upon the ranges seen within the HEDs. The largest error bar for Vestoid band center calculations is shown (±0.005 μm for band 2, band 1 center errors are within the scale of the symbols). The Vestoid band centers predominantly overlap the howardite field, with a few spectra also in the eucrite and diogenite fields. A few eucrite samples have band centers that extend the eucrite field into longer wavelengths. They were omitted from this diagram for clarity. 2511 Patterson is highlighted in this diagram as it can be modeled using a one-pyroxene model and yet has band centers at much longer wavelengths than most diogenites. 2511 Patterson is likely a ferroan diogenite asteroid and would be expected to have a similar mineralogy to that of Y-75032 shown in part (a) of this figure.

In HCP–LCP mixtures the presence of olivine is better detected by the presence of a longer wavelength 1-μm feature (Gaffey et al., 2002). An olivine-bearing Vestoid would be offset in a plot comparing continuum-removed bands 1 and 2 centers. This is not seen for any of the samples including three of those identified to have ~30% olivine by Duffard et al. (2004)(Fig. 5b). This is further supported by MGM analyses of the 15 Vestoids, which do not require bands suggestive of olivine to achieve a good fit. There are two possibilities to explain the lack of olivine in any of the Vestoid spectra: the south-pole excavation identified by Thomas et al. (1997) did not sample a significant amount of upper mantle material; the assumption that Vesta's upper mantle consists of an olivine-rich lithology is incorrect. Asteroid differentiation is far from being completely understood and, while the majority of models favor the formation of a dunite mantle (e.g. Mason, 1962; Ruzicka et al., 1997), there are others that have suggested alternative asteroidal mantle materials such as harzburgite (Righter and Drake, 1997; Beck and McSween, 2010), high-Ca pyroxene rich cumulates (Thomas et al., 1997), and even a relict layer of highly metamorphosed chondritic material (McCoy et al., 2006).

5. Implications for the surface of Vesta

One of the major goals of the Dawn mission is to provide a geologic context for HED meteorites. The results will be limited both by the resolution of the instruments and the sizes of individual rock-units on the surface. The highest resolution geologic map currently available for the surface of Vesta was generated using the rotational variations in its spectra from Hubble Space Telescope data, with a resolution of 52 km/pixel (Binzel et al., 1997). Therefore, our knowledge of the variation on the surface is limited at present. The presence of regions with dominant eucrite and dominant diogenite components has been suggested (Gaffey, 1997), and olivine signatures have been suggested within the large crater in the south-pole region of Vesta (Gaffey, 1997; Binzel et al., 1997). In advance of Dawn's arrival at Vesta, Vestoids provide a means of examining the scale of variability vertically and laterally within Vesta's crust, offering clues to the mechanisms behind its formation.

The Vestoid spectral dataset (Fig. 1) does not show the same spectral variation seen within the HED meteorite spectra (Figs. 2–4). Subtle features such as the 0.6-μm and 1.2-μm band are all but absent in the Vestoid spectra and band centers, widths, and depths are much more homogeneous. This can be best explained by invoking space-weathering processes on the surface of the Vestoids, which is known to diminish band depth in the VIS–NIR range (Chapman, 2004 and references therein). Previous authors have also noted that the Vestoid spectra tend to be much redder than that of the HEDs and Vesta (Hiroi and Pieters, 1997, 1998; Burbine et al., 1998; Shestopalov and Golubeva, 2008), which is another prime indicator of space weathering.

Table 5
Modified Gaussian bands required in the MGM fits for the HEDs and Vestoids.

	Absorption	ALH A8100I BE	BTN 00300 BE	Chervony Kut BE	EET 87520 BE	GRA 98098 BE	Ibitira BE	MAC 02522 BE	MET 01081 BE	Moore Country CE	PCA 9I078 BE	Serra de Mage CE	EET 87503 H	QUE 94200 H	Y-791573 H	EET A79002 D	LAP 91900 D	GRO 95555 D
Band 1	Charge transfer	Y	Y	Y	Y	Y	Y	Y	Y	Y	Y	Y	Y	Y	Y	Y	Y	Y
Band 2	Charge transfer	Y	Y	Y	Y	Y	Y	Y	Y	Y	Y	Y	Y	Y	Y	Y	Y	Y
Band 3	Cr^{3+}	Y	Y	Y	Y	Y	Y	Y	Y	Y	Y	Y	Y	Y	Y	Y	Y	Y
Band 4	1 μm MI	N	Y	Y	N	N	N	Y	N	N	N	N	N	N	N	N	N	N
Band 5	LCP 1 μm	N/A*	Y	Y	Y	Y	Y	N/A*	Y	Y	Y	Y	Y	Y	Y	N/A*	N/A*	N/A*
Band 6	HCP 1 μm	N/A*	Y	Y	Y	Y	Y	N/A*	Y	Y	Y	Y	Y	Y	Y	N/A*	N/A*	N/A*
Band 7	1.2 μm	Y	Y	Y	Y	Y	Y	Y	Y	Y	Y	Y	Y	Y	Y	Y	Y	Y
Band 8	LCP 2 μm	N/A*	Y	Y	Y	Y	Y	N/A*	Y	Y	Y	Y	Y	Y	Y	N/A*	N/A*	N/A*
Band 9	HCP 2 μm	N/A*	Y	Y	Y	Y	Y	N/A*	Y	Y	Y	Y	Y	Y	Y	N/A*	N/A*	N/A*
Band 10	Water band	Y	Y	Y	Y	Y	Y	Y	Y	Y	Y	Y	Y	Y	Y	Y	Y	Y

	Absorption	1929 Kollaa	2045 Pecking	2511 Patterson	2566 Kirghizia	2579 Spartacus	2653 Principia	2763 Jeans	2795 Lepage	2851 Harbin	2912 Lapalma	3155 Lee	3782 Celle	3908 Nyx	4188 Kitezh	4215 Kamo
Band 1	Charge transfer															
Band 2	Charge transfer	Y	Y	Y	Y	Y	Y	Y	Y	Y	Y	Y	Y	Y	Y	Y
Band 3	Cr^{3+}	Y	Y	Y	Y	Y	Y	Y	Y	Y	Y	Y	Y	Y	Y	Y
Band 4	1 μm M1	N	N	N	N	N	N	N	N	N	N	Y	Y	N	N	N
Band 5	LCP 1 μm	Y	Y	N/A*	Y	Y	Y	Y	Y	N/A*	Y	N/A*	N/A*	Y	Y	N/A*
Band 6	HCP 1 μm	Y	Y	N/A*	Y	Y	Y	Y	Y	N/A*	Y	N/A*	N/A*	Y	Y	N/A*
Band 7	1.2 μm	Y	Y	Y	Y	Y	Y	Y	Y	Y	Y	Y	Y	Y	Y	Y
Band 8	LCP 2 μm	Y	Y	N/A*	Y	Y	Y	Y	Y	N/A*	Y	N/A*	N/A*	Y	Y	N/A*
Band 9	HCP2 μm	Y	Y	N/A*	Y	Y	Y	V	Y	N/A*	Y	N/A*	N/A*	Y	Y	N/A*
Band 10	Water band	Y	Y	Y	Y	Y	Y	Y	Y	Y	Y	Y	Y	Y	Y	Y

N/A* for band numbers 5, 6 and 8, 9 denotes eucrites that only needed one pyroxene in the model and, therefore, instead of separate LCP and HCP bands only one pyroxene band was needed in both the 1 and 2 μm regions.
BE = basaltic eucrite, CE = cumulate eucrite, H = howardite, D = diogenite.

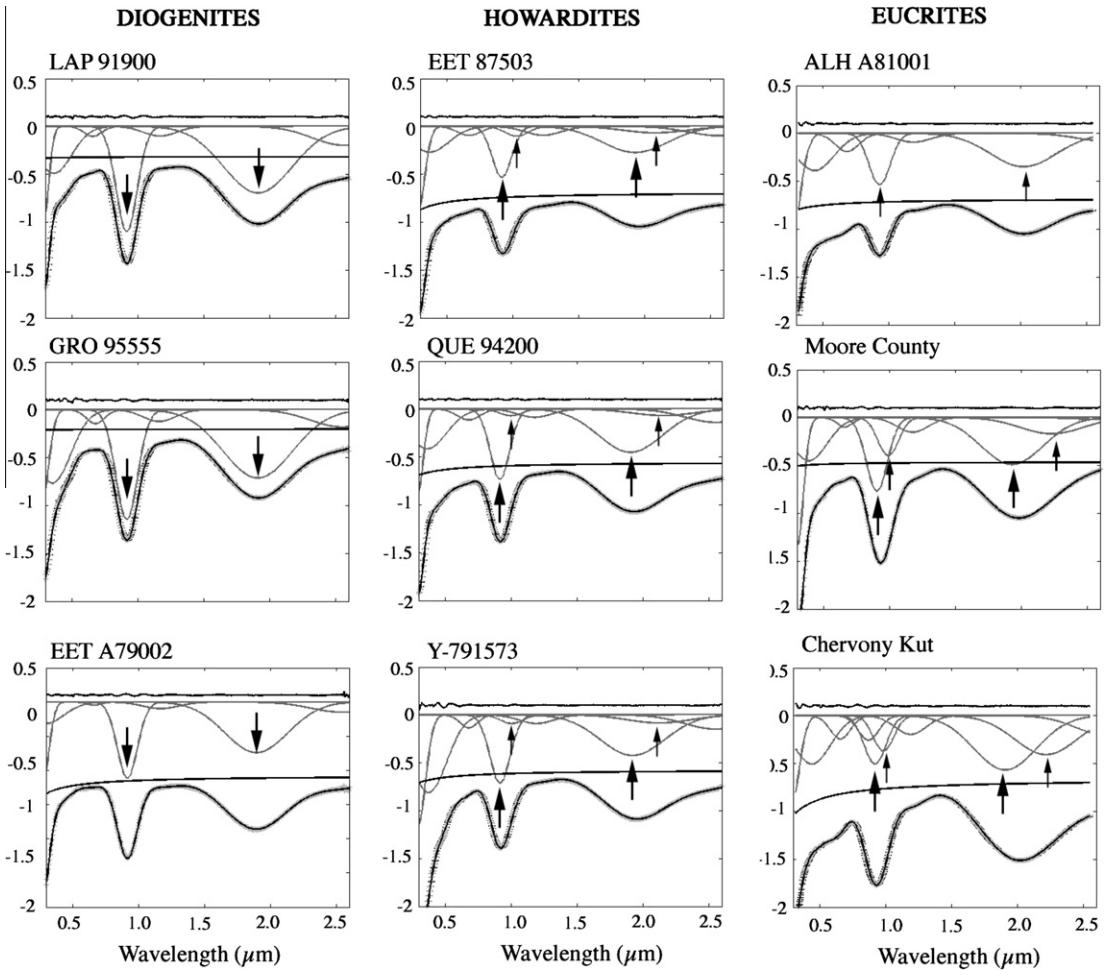

Fig. 6. MGM fits for the howardites, diogenites, and three selected eucrites from Mayne et al. (2010). The eucrite spectra chosen show the range of spectral features seen within the group. The individual absorption bands modeled by modified Gaussians are shown in dark gray. The upper black line represents the residual error of the model; the lower black line represents the continuum. The measured spectrum is plotted with gray +'s, and the black is the modeled value. A large arrow is used to denote the LCP band in the 1 and 2-μm region, and a small arrow for HCP in the howardites. All diogenites are fit well with a one-pyroxene model and, therefore, only have one LCP band in both the 1 and 2-μm region, whereas both the howardites and eucrites have two-pyroxenes. It can be seen that all spectra have a 1.2-μm band in the model fit.

Of the 15 Vestoids studied, eight asteroids appear to represent mixtures of eucrite and diogenite, which could suggest any one, or a mixture, of three different possibilities.

1. *Vestoids dominated by howardite material*: Vestoids spectrally similar to howardites on a hemispheric scale could, in fact, be dominated by finely-mixed howardite material. There are several arguments against this suggestion. Firstly, only 15% of the HED meteorites by mass have been classified as howardites (Burbine et al., 2001), and as the Vestoids are believed to be the delivery pathway for the HED meteorites, it would then seem likely that this number would be higher if they were primarily howardites themselves. More importantly, for the Vestoids to be composed of primarily howardite material, the regolith on Vesta would have to be a mixed-megaregolith on the scale of 5–8 km. This depth of regolith, which is several orders of magnitude greater than that predicted for the lunar regolith (e.g. Quaide and Oberbeck, 1968; Cooper et al., 1974; Wilcox et al., 2005), seems unlikely.
2. *Asteroidal rubble piles*: The processes of impact excavation and ejection of material are key to the formation of the Vestoids. It is possible that the majority of the Vestoids are, in fact, re-accumulated piles of homogenized rock, effectively howardite rubble piles that formed after their ejection from the surface of Vesta. This mechanism was suggested by Michel et al. (2001) as a way to produce asteroidal families. This could not be a universal process or there would not be Vestoids that appear to consist entirely of eucrite or diogenite material.
3. *Surface heterogeneity*: Eight of the fifteen Vestoids have spectra that indicate that both diogenite and eucrite material is present. It is possible that the spectra sample hemispherically averaged compositions of distinct terrains, meaning the asteroid is made up of distinct areas of pure-eucrite and pure-diogenite as opposed to being a howardite. If this is the case, then we know that the size of each individual lithology (the eucrite-only and diogenite-only regions) contributing to the averaged composition must be smaller than the surface being measured. 3908 Nyx, at less than 1 km in diameter, is the smallest Vestoid in this study, suggesting that mixing is present on a sub-kilometer scale. This could indicate that there are areas on Vesta with smaller-scale heterogeneity.

The seven remaining Vestoids are dominated by diogenitic or eucritic material, supporting the idea of large essentially mono-lithologic units in Vesta's crust, although each unit could be polymict, i.e. a mixture of different eucrite or different diogenite materials. The existence of these domains, greater than 5 km in size (Table 6), implies large-scale lateral and vertical homogeneity in Vesta's crust.

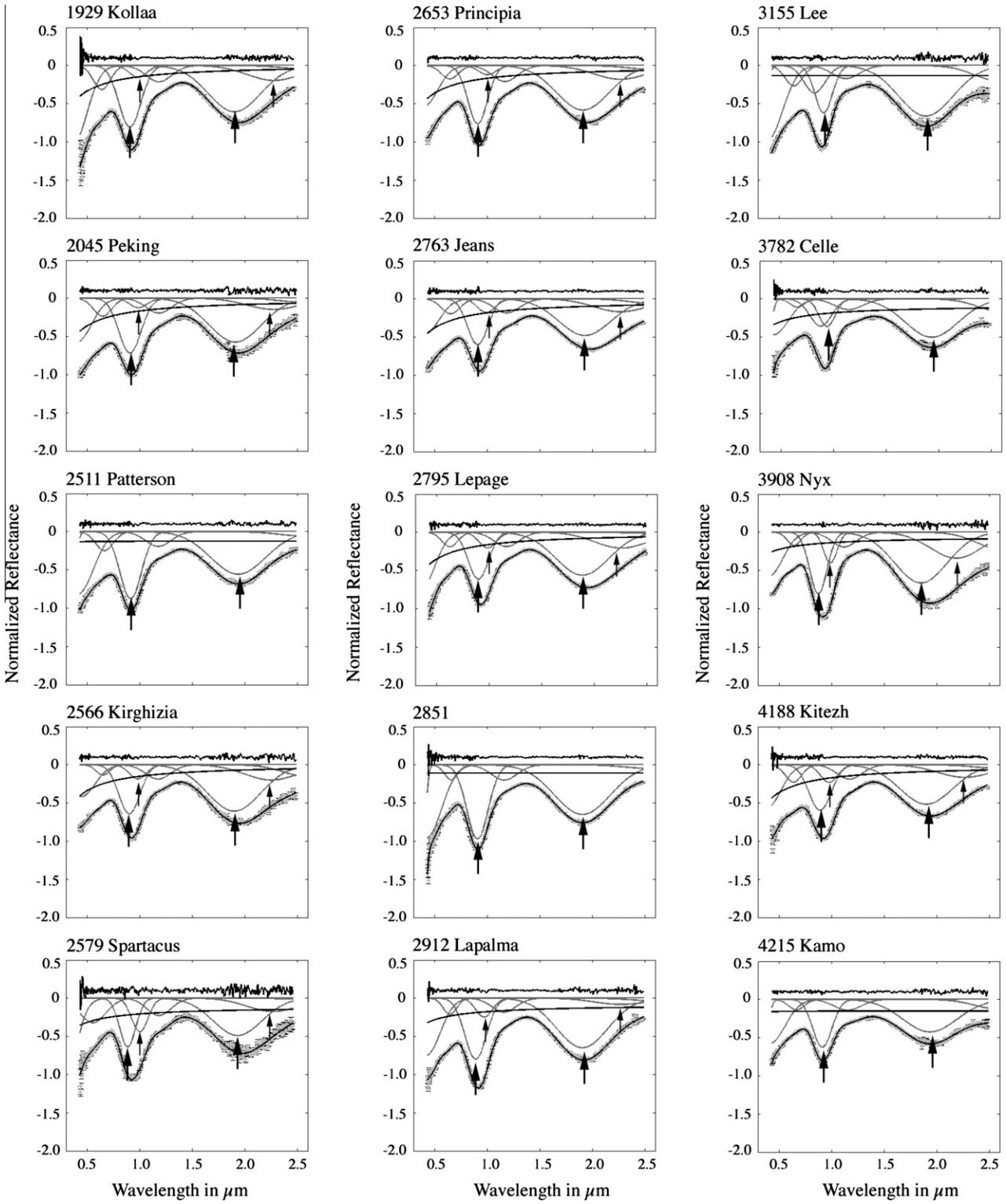

Fig. 7. MGM model fits of the Vestoids. The individual absorption bands modeled by modified Gaussians are shown in dark gray. The upper black line represents the residual error of the model; the lower black line represents the continuum. The measured spectrum is plotted with gray +'s, and the black is the modeled value. A large arrow is used to denote the LCP band in the 1 and 2-μm region, and a small arrow for HCP.

5.1. What can the scale of heterogeneity tell us about the origin of Vesta's crust?

The formation of Vesta is not well understood and numerous models have been put forward, with partial melting and a magma ocean remaining the two most prevalent (e.g. Mason, 1962; Stolper, 1977; Righter and Drake, 1997; Ruzicka et al., 1997). Remotely sensed data of both Vesta and the Vestoids offer the opportunity to test these models, with respect to the units exposed on their surface.

The magma-ocean formation model (Righter and Drake, 1997; Ruzicka et al., 1997) predicts large-scale homogeneity both

Table 6
Size and suggested mineralogy for the Vestoids.

Vestoids	1.2 μm feature visible	MGM model # of pyroxenes	Diameter (km)	Band 1 center (μm)	Band 2 center (μm)	Suggested mineralogy
3155 Lee	N	1	6.2	0.9152 ± 0.001	1.896 ± 0.002	Diogenite
2851 Harbin	N	1	7.1	0.923 ± 0.001	1.9151 ± 0.002	Diogenite
3908 Nyx	N	2	0.7	0.924 ± 0.001	1.926	Mixture
4215 Kamo	N	1	6.8	0.925 ± 0.002	1.930 ± 0.002	Diogenite
2912 Lapalma	N	2	5.9	0.926	1.928 ± 0.004	Mixture
3782 Celle	N	1	6.5	0.927	1.9232 ± 0.002	Diogenite
2511 Patterson	N	1	6.5	0.929	1.9424 ± 0.002	Diogenite
2566 Kirghizia	Y	2	6.2	0.933	1.938 ± 0.003	Mixture
2795 Lepage	Y	2	4.7	0.933 ± 0.001	1.946 ± 0.002	Mixture
2653 Principia	Y	2	7.8	0.933	1.951 ± 0.001	Mixture
4188 Kitezh	N	2	5.9	0.934	1.9417 ± 0.003	Mixture
1929 Kollaa	Y	2	7.4	0.935 ± 0.003	1.940 ± 0.002	Mixture
2045 Peking	Y	2	7.4	0.936	1.950 ± 0.004	Mixture
2763 Jeans	Y	2	6.2	0.940	1.976 ± 0.002	Eucrite
2579 Spartacus	Y	2	5.2	0.940 ± 0.001	1.985 ± 0.005	Eucrite

Vestoids are in order of band 1 center values, starting with the shortest.
Diameter was calculated using the formula from Chesley et al. (2002), where $D \sim 1329\ \text{km} \times 10^{-H/5\rangle v-1/2}$, where H = absolute magnitude, $\rangle$ = visual albedo, taken to be 0.42 (Vesta's Infrared Astronomical Satellite albedo). Values of H were taken from the JPL small-body database.
The uncertainty in band centers is given to three decimal places and, if not given, was calculated to be zero.

laterally and with depth. The eucrites and diogenites are formed as separate layers and mixing of the two by intrusions would be minimal. The models predict different thicknesses for each layer depending on the mode of crystallization used. Ruzicka et al. (1997) calculated that fractional crystallization of a magma ocean would result in a 23–42 km thick mafic crust (eucrites) with a 12–43 km thick orthopyroxenites layer (diogenites) beneath it. In contrast, an equilibrium crystallization model which switches to fractional crystallization after convective lock-up suggests a 10–15 km thick basaltic crust, with the thickness of the orthopyroxenites (diogenite) layer varying depending on when the switch to fractional crystallization occurred (Righter and Drake, 1997; McCoy et al., 2006). The Vestoids studied here are all less than 10 km in size and, therefore, if the magma ocean models were correct we would expect to see predominantly single lithology asteroids, with perhaps a few exhibiting a mixture of eucrite and diogenite reflecting rubble piles or howarditic material.

What is actually observed amongst the Vestoids is evidence of both large-scale (>5 km) homogeneity (just eucrite or diogenite) and small-scale (~1 km) heterogeneity (eucrite and diogenite) on their surface, representing changes both laterally and vertically within Vesta. It is hard to envisage how this apparent widespread mixing could occur on such a small-scale within the magma ocean model. The mixture of widespread (>5 km) and localized (~1 km) units observed within the Vestoids seems to better fit with the partial melting model for the formation of Vesta. Partial melting models allow for greater heterogeneity (Ghosh and McSween, 1998; McCoy et al., 2006). Multiple intrusions of basaltic melts are predicted to occur both at shallow depths (<10 km vertical height, <1 km wide) and at depth (<30 km lateral extent, <3 m thickness) (Wilson and Keil, 1996).

If the partial melting model is correct then it must be able to explain the formation of large (>5 km) ferroan diogenite regions within the crust of Vesta, shown in this study by 2511 Patterson. There are two main mechanisms suggested for the formation of ferroan diogenites: that they formed from different parental melts relative to the more typical Mg-rich diogenites (Yamagchi et al., 2009); they are produced late in a sequence of fractional crystallization within individual magma chambers (Beck and McSween, 2010). Both of these formation mechanisms are possible within the partial melting model for Vesta. The modeled spectra of 2511 Patterson indicates that diogenitic magma chambers within Vesta's crust must have had considerable lateral and vertical extent. If the ferroan diogenites are formed from separate parental melts then magma chambers of over 6 km in diameter (both width and depth) are required. If the ferroan diogenites represent the end-product of a diogenite fractional crystallization sequence, then 2511 Patterson is reflecting the composition of the upper layers of what was a much more massive, layered igneous intrusion.

6. Summary

(1) The mineralogy and LCP:HCP ratios of 14 Vestoid spectra and 1 V-type spectrum were analyzed and compared to HED meteorite spectra using their continuum-removed band centers and the Modified Gaussian Model.
(2) Seven of the 15 spectra were modeled using only one HED meteorite type, i.e. were composed of all eucrite of diogenite. 3155 Lee, 2851 Harbin, 4215 Kamo, 3782 Celle, and 2511 Patterson were all fit well using a diogenite model of one low-Ca pyroxene. 2763 Jeans and 2579 Spartacus have continuum-removed band centers and a calculated LCP:HCP ratio equivalent to those of the basaltic eucrites. These asteroids, all over 5 km in size, suggest that large-scale (>5 km) homogeneity both laterally and vertically is present at Vesta.
(3) The eight remaining Vestoids that were interpreted to contain a mixed eucrite and diogenite spectrum could be rubble piles, dominated by howardite material, or reflect actual surface heterogeneity inherited from Vesta. Whilst impact processes may play a role in producing mixed lithology Vestoids, the presence of mono-lithologic members confirms they are not dominant, and it is unlikely that the regolith on Vesta is thick enough to produce intact howardite ejecta blocks of up to 8 km. Therefore, it seems clear that a large proportion of the 'mixed' Vestoids are reflecting the petrologic variation on Vesta.
(4) Current magma ocean models do not predict heterogeneity at the small-scale seen within the Vestoids; instead they seem to support the theory that partial melting may have played a significant role in the petrogenesis of Vesta.
(5) 2511 Patterson is proposed to be of ferroan diogenite composition and is the first asteroid of its type to be identified. According to the current models for ferroan diogenite petrogenesis, the 6.5 km asteroid either represents an individual magma chamber, or the upper portion of a much more massive, layered, diogenite intrusion. Either model speaks to the large-scale processes that occurred during the differentiation of Vesta itself.

Acknowledgments

This work was supported by PGG Grant NNX06AH69G to J.M.S., a NASA Cosmochemistry Grant NNG06GG36G to T.J.M. and UCLA subcontract 2090-S-JB694 for Dawn to H.Y.M. All meteorite spectra were collected at Brown University's KECK/NASA Reflectance Experiment Laboratory (RELAB).

References

Beck, A., McSween, H.Y., 2010. Diogenites as polymict breccias composed of orthopyroxene and harzburgite. Meteor. Planet. Sci. 45, 850–872.
Binzel, R.P., Xu, S., 1993. Chips off asteroid 4 Vesta: Evidence for the parent body of basaltic achondrite meteorites. Science 260, 186–191.
Binzel, R.P., Gaffey, M.J., Thomas, P.T., Zellner, B.H., Storrs, A.D., Wells, E.N., 1997. Geologic mapping of Vesta from 1994 Hubble Space Telescope images. Icarus 128, 95–103.
Burbine, T.H., Binzel, R.P., Bus, S.J., 1998. Is Vesta the parent body of the "Vesta Chips"? Yes. Lunar Planet. Sci. 29. Abstract #1459 (CD-ROM).
Burbine, T.H., Buchanan, P.C., Binzel, R.P., Bus, S.J., Hiroi, T., Hinrichs, J.L., Meibom, A., McCoy, T.J., 2001. Vesta, Vestoids, and the howardite, eucrite, diogenite group: Relationships and the origin of spectral differences. Meteor. Planet. Sci. 36, 761–781.
Burbine, T.H., Buchanan, P.C., Dolkat, T., Binzel, R.P., 2009. Pyroxene mineralogies of near-Earth Vestoids. Meteor. Planet. Sci. 44, 1331–1341.
Burns, R.G., 1993. Mineralogical Applications of Crystal Field Theory, second ed. Cambridge University Press, New York, 551 p.
Bus, S.J., Binzel, R.P., 2002. Phase II of the small main-belt asteroid spectroscopic survey: A feature based taxonomy. Icarus 158, 146–177.
Chapman, C.R., 2004. Space weathering of asteroid surfaces. An. Rev. Earth Planet. Sci. 32, 539–567.
Chesley, S.R., Chodas, P.W., Miliani, A., Valseechi, G.B., Yeomars, D.K., 2002. Quantifying the risk posed by potential Earth impacts. Icarus 159, 423–432.
Cloutis, E.A., Gaffey, M.J., Jackowski, T., Reed, K.J., 1986. Calibrations of phase abundance, composition, and particle size distribution for olivine–orthopyroxene mixtures from reflectance spectra. J. Geophys. Res. 95, 8323–8338.
Cooper, M.R., Kovach, R.L., Watkins, J.S., 1974. Lunar near-surface structure. Rev. Geophys. Space Phys. 12, 291–308.
Duffard, R., Lazarro, D., Licandro, J., De Sanctis, M.C., Capria, M.T., Carvano, J.M., 2004. Mineralogical characterization of some basaltic asteroids in the neighborhood of (4) Vesta: First results. Icarus 171, 120–132.
Gaffey, M.J., Bell, J.F., Brown, R.H., Burbine, T.H., Piatek, J.L., Reed, K.L., Chaky, D.A., 1993. Mineralogic variations within the S-type asteroid class. Icarus 106, 573–602.
Gaffey, M.J., 1997. Surface lithologic heterogeneity of asteroid 4 Vesta. Icarus 127, 130–157.
Gaffey, M.J., Cloutis, E.A., Kelley, M.S., Reed, K.L., 2002. Mineralogy of the asteroids. In: Bottke, W.F., Cellino, A., Paolicchi, P., Binzel, R.P. (Eds.), Asteroids III. University of Arizona, Tucson, pp. 183–204.
Ghosh, A., McSween, H.Y., 1998. A thermal model for the differentiation of asteroid 4 vesta, based on radiogenic heating. Icarus 134, 187–206.
Hinrichs, J.L., Lucey, P.G., Robinson, M.S., Meibom, A., Krot, A.N., 1999. Implications of temperature-dependent near-IR spectral properties of common minerals and meteorites for remote sensing of asteroids. Geophys. Res. Lett. 26, 1661–1664.
Hiroi, T., Pieters, C.M., 1998. Origin of Vestoids suggested from the space weathering trend in the visible reflectance spectra of HED meteorites and lunar soils. Antarct. Meteor. Res. 11, 163–170.
Kanner, L.C., Mustard, J.F., Gendrin, A., 2007. Assessing the limits of the Modified Gaussian Modal for remote spectroscopic studies of pyroxenes on Mars. Icarus 187, 442–456.
Kelley, M.S., Vilas, F., Gaffey, M.J., Abell, P.A., 2003. Quantified mineralogy evidence for a common origin of 1929 Kollaa with 4 Vesta and the HED meteorites. Icarus 165, 215–218.
Klima, R.L., Pieters, C.M., Dyar, M.D., 2007. Spectroscopy of synthetic Mg–Fe pyroxenes I: Spin-allowed and spin-forbidden crystal field bands in the visible and near-infrared. Meteor. Planet. Sci. 42, 235–253.
Klima, R.L., Pieters, C.M., Dyar, M.D., 2008. Characterization of the 1.2-μm M1 pyroxene band: Extracting cooling history from near-IR spectra of pyroxenes and pyroxene-dominated rocks. Meteor. Planet. Sci. 43, 1591–1604.
Lazzaro, D., Michtchenko, T., Carvano, J.M., Binzel, R.P., Bus, S.J., Burbine, T.H., Mothe-Diniz, T., Florczak, M., Angeli, C.A., Harris, A.W., 2000. Discovery of a basaltic asteroid in the outer main belt. Science 288, 2033–2035.
Lord, S.D., 1992. NASA Technical Memorandum 103957.
Marzari, F., Cellino, A., Davis, D., Farinella, P., Zappala, V., Vaanzani, V., 1996. Origin and evolution of the vesta asteroid family. Astron. Astrophys. 316, 248–262.
Mason, B., 1962. Meteorites. J. Wiley and Sons, New York.
Mayne, R.G., McSween, H.Y., McCoy, T.J., Gale, A., 2009. Petrology of the unbrecciated eucrites. Geochim. Cosmochim. Acta. 73, 794–819.
Mayne, R.G., Sunshine, J.M., McSween, H.Y., McCoy, T.J., Corrigan, C.M., Gale, A., Dyar, M.D., 2010. Spectra of the unbrecciated eucrites. Meteor. Planet. Sci. 45, 1074–1092.
McCord, T.B., Adams, J.B., Johnson, T.V., 1970. Asteroid Vesta: Spectral reflectivity and compositional implications. Science 168, 144–1445.
McCoy, T.J., Mittlefehldt, D.W., Wilson, L., 2006. Asteroid differentiation. In: Lauretta, D.D., McSween, H.Y. (Eds.), Meteorites and the Early Solar System. University of Arizona Press, pp. 733–745.
Michel, P., Benz, W., Tanga, P., Richardson, D.C., 2001. Collisions and gravitational reaccumulation: Forming asteroid families and satellites. Science 294, 1696–1700.
Mittlefehldt, D.W., Lindstrom, M.M., 2003. Geochemistry of eucrites: Genesis of basaltic eucrites, and Hf and Ta as petrogenetic indicators for altered Antarctic eucrites. Geochim. Cosmochim. Acta 67, 1911–1935.
Moroz, L., Schade, U., Wäsch, R., 2000. Reflectance spectra of olivine–orthopyroxene bearing assemblages at decreased temperatures: Implications for remote sensing of asteroids. Icarus 147, 79–93.
Moskovitz, N.A., Willman, M., Burbine, T.H., Binzel, R.P., Bus, S.J., 2010. A spectroscopic comparison of HED meteorites and V-type asteroids in the inner main-belt. Icarus 208, 773–788.
Mustard, J.F., 1992. Chemical analysis of actinolite from reflectance spectra. Am. Min. 77, 345–358.
Nesvorny, D., Bottke, W.F., Vokrouhlicky, D., Morbidelli, A., Jedicke, R., 2006. Asteroid families. In: Lazzaro, D., Ferraz-Mello, S., Fernandez, J.A. (Eds.), Asteroids, Comets, Meteors – Proceedings IAU Symposium No. 229. Cambridge University Press, pp. 289–299.
Pieters, C.M., 1983. Strength of mineral absorption features in the transmitted component of near-infrared reflected light: First results from RELAB. J. Geophys. Res. 88, 9534–9544.
Pieters, C.M., Hiroi, T., 2004. RELAB (Reflectance Experiment Laboratory): A NASA multi-user spectroscopy facility. Lunar Planet. Sci. 35. Abstract #1720 (CD-ROM).
Quaide, W.L., Oberbeck, V.R., 1968. Thickness determinations of the lunar surface layer from lunar impact craters. J. Geophys. Res. 73, 5247–5270.
Rayner, J.T., Toomey, D.W., Onaka, P.M., Denault, A.J., Stahlberger, W.E., Vacca, W.D., Cushing, M.C., Wang, S., 2003. SpeX: A medium resolution 0.8–5.5 μm spectrograph and imager for the NASA Infra-red telescope facility. Pub. Astro. Soc. Pacific 115, 362–382.
Righter, K., Drake, M.J., 1997. A magma ocean on Vesta: Core formation and petrogenesis of eucrites and diogenites. Meteor. Planet. Sci. 32, 244–929.
Roig, F., Nesvorny, D., Gil-Hutton, R., Lazzaro, D., 2008. V-type asteroids in the middle main-belt. Icarus 194, 125–136.
Rothman, L.S. et al., 2005. The HITRAN 2004 moecular spectroscopic database. J. Quant. Spectrosc. Ra. 96, 139–204.
Roush, T.L., Singer, R.B., 1987. Possible temperature variation effects on the interpretation of spatially resolved reflectance observations of asteroid surfaces. Icarus 69, 571–574.
Ruzicka, A., Synder, G.A., Taylor, L.A., 1997. Vesta as the howardite, eucrite, and diogenite parent body: Implications for the size of a core and for large-scale differentiation. Meteor. Planet. Sci. 32, 825–840.
Schade, U., Wäsch, R., 1999a. Near-infrared reflectance spectroscopy if mafic minerals in the temperature region between 80 and 473 K. Adv. Space Res. 23, 1253–1256.
Schade, U., Wäsch, R., 1999b. Near-infrared reflectance spectra from bulk samples of the two SNC meteorites Zagami and Nakhla. Meteor. Planet. Sci. 34, 417–424.
Shestopalov, D., Golubeva, L., 2008. Why Vesta's surface is unweathered. Lunar Planet. Sci. 39. Abstract #1116 (CD-ROM).
Singer, R.B., Roush, T.L., 1985. Effects of temperature on remotely sensed mineral absorption features. J. Geophys. Res. 90, 12434–12444.
Stolper, E., 1977. Experimental petrology of eucritic meteorites. Geochim. Cosmochim. Acta 41, 587–611.
Storm, S., Bus, S.J., Binzel, R.P., 2007. Olivine–pyroxene distribution of S-type asteroids in the main belt. B. Am. Astro. Soc. 39, 448 (abstract).
Sunshine, J.M., Pieters, C.M., 1993. Estimating modal abundances from the spectra of natural and laboratory pyroxene mixtures using the Modified Gaussian Model. J. Geophys. Res. 98, 9075–9087.
Sunshine, J.M., Pieters, C.M., Pratt, S.F., 1990. Deconvolution of mineral absorption bands: An improved approach. J. Geophys. Res. 95, 6955–6966.
Sunshine, J.M., Bus, S.J., McCoy, T.J., Burbine, T.H., Corrigan, C.M., Binzel, R.P., 2004. High-calcium pyroxene as an indicator of igneous differentiation in asteroids and meteorites. Meteor. Planet. Sci. 39, 1343–1357.
Tholen, D., Barucci, M.A., 1989. Asteroid taxonomy. In: Binzel, R.P., Gerhels, T., Matthews, M.S. (Eds.), Asteroids II. University of Arizona, Tucson.
Thomas, P.C., Binzel, R.P., Gaffey, M.J., Storrs, A.R., Wells, E.N., Zellner, B.H., 1997. Impact excavation on asteroid 4 Vesta: Hubble Space Telescope results. Science 277, 1492–1495.
Wilcox, B.B., Robinson, M.S., Thomas, P.C., Hawke, B.R., 2005. Constraints on the depth and variability of the lunar regolith. Meteor. Planet. Sci. 40, 695–710.
Wilson, L., Keil, K., 1996. Volcanic eruptions and intrusions on the asteroid 4 Vesta. J. Geophys. Res. 101, 18927–18940.
Yamagchi, A., Takeda, H., Barrat, J.A., 2009. Petrology of ferroan diogenite, Yamato 75032 type, Asuka 881839, and Dhofar 700. Lunar Planet. Sci. 40. Abstract #1547 (CD-ROM).
Zappalà, V., Bendjoya, P., Cellino, A., Farinella, P., Froeschlé, C., 1995. Asteroid families: Search of a 12,487-asteroid sample using two different clustering techniques. Icarus 116, 291–314.